Non-Contact Dielectric Spectroscopy of Multi-Layered Substrates Towards Organ-on-Chip Applications

Hosman, Tim; Mastrangeli, Massimo; Spirito, Marco

DOI
10.1109/JERM.2025.3538953

Publication date
2025

Document Version
Final published version

Published in
IEEE Journal of Electromagnetics, RF and Microwaves in Medicine and Biology

Non-Contact Dielectric Spectroscopy of Multi-Layered Substrates: Towards Organ-on-Chip Applications

Tim Hosman, Massimo Mastrangeli, *Member, IEEE*, and Marco Spirito, *Member, IEEE*

***Abstract*—Dielectric spectroscopy is a label-free, non-contact, real-time, multi-layer sensing technology, and has been used for identification and quantification of many biological materials. A combination of such sensing features is in demand for monitoring of organ-on-chip systems; however available sensing technologies have yet to address this need. In this work, we explore the possibility of leveraging the inherent features of dielectric spectroscopy for the application in organ-on-chip systems, by investigating three key technological developments using open-ended coaxial probes. Firstly, biocompatible non-contact sensing capabilities are proved by showing similar sensing performance of Parylene C-coated probes and uncoated probes. Secondly, a setup and methodology are developed for highly accurate and non-destructive height positioning of the probe to allow for precise extraction of intermediate sample layers. Finally, non-contact multi-layer sensing performance of the presented technology is successfully demonstrated by means of a biological phantom in a three-layered system. With further integration, dielectric spectroscopy can potentially become a cornerstone sensing technique for organ-on-chip by enabling real-time non-contact tracking of various tissue contents and properties.**

***Index Terms*—Dielectric spectroscopy, label-free, micro-physiological systems, non-contact, open-ended coaxial probe, organ-on-chip, proof-of-principle, reflectometer, sensing, single-layer extraction.**

I. Introduction

DIELECTRIC spectroscopy (DS) is a well-established sensing technique to characterise a material's response, by means of its complex permittivity, to an electric field at various frequencies. The dielectric spectrum is unique for each type of molecule, acting as a specific label-free fingerprint which allows for the identification and quantification of the material composition [1], [2]. As such, DS has been used in the characterisation of different biological materials [3], thereby also in in vivo and in vitro applications, such as sensing of proteins, biomarkers, glucose and various cell properties [1], [4], [5], [6]. Open-ended coaxial probes (OECPs) and planar transmission lines are among the most used broadband and non-destructive sensing devices for DS in biological applications [7]. These devices make use only of a vector network analyser (VNA) to extract the frequency response of the biological material under investigation with high measurement sensitivity and without requiring presence of labelling agents in the biological target [1], [8], [9]. In contrast to most conventional non-contact monitoring techniques, such as fluorescent microscopy, DS can be executed in real-time without experiment termination, thus allowing for non-contact tracking of specific cell contents and processes over time [5]. More generally, DS can provide unique insights in biological processes where conventional techniques are either bulky (e.g. MRI and X-ray), terminative (e.g. fluorescence microscopy), lacking in contrast (e.g. optical microscopy), limited to geometry sensing (e.g. optical coherence microscopy) or invasive (e.g. 2D/3D impedance spectroscopy) [8], [10], [11].

Planar DS systems, with the inclusion of microfluidic channels, have become the configuration of choice to characterise cells suspended in their biological medium or to analyse single cells [12]. On the other hand, OECPs have been chosen in the presence of more complex biological matter (i.e., tissues) [13], requiring minimal sample preparation and capable of optimised sensing depth when measuring heterogeneous tissue by simply varying the probe aperture size [14].

Despite its advantages, DS has yet to find a correspondingly wide application in monitoring of micro-physiological systems. Organ-on-chip (OoC) has emerged over the last decade as a micro-physiological technology capable of increasingly relevant modelling of small scale human organs [15]. OoC aims for more reliable (and thus more affordable [16]) pre-clinical drug testing, effective personalised medicine and alleviation of the ethical burden of animal-based drug studies [15], [17], [18]. Integrated sensing in OoC is vital for its success, as it enables repeatable quantification and dynamic tracking of standard tissue properties [15]. Notably, one of the main unmet needs of OoC is time-continuous non-contact monitoring of microenvironments [15], [18], [19], a niche for which DS could be an excellent candidate considering its mentioned inherent features. Acting as a founding proof-of-principle, this work investigates the capability of using OECP-based DS for OoC in a simplified characterisation setup (see Fig. 1(a)), and aims to pave the road to full integration of DS in OoC systems (see Fig. 1(b)–(c)). In order to enable DS sensing capabilities in OoC application, three key technological developments, addressed in this work, need to take place:

Received 22 October 2024; revised 20 January 2025; accepted 1 February 2025. Date of publication 27 February 2025; date of current version 25 August 2025. *(Corresponding author: Tim Hosman.)*

The authors are with the Department of Microelectronics, Delft University of Technology, 2628 CD Delft, The Netherlands (e-mail: t.b.hosman@tudelft.nl; m.mastrangeli@tudelft.nl; m.spirito@tudelft.nl).

Digital Object Identifier 10.1109/JERM.2025.3538953

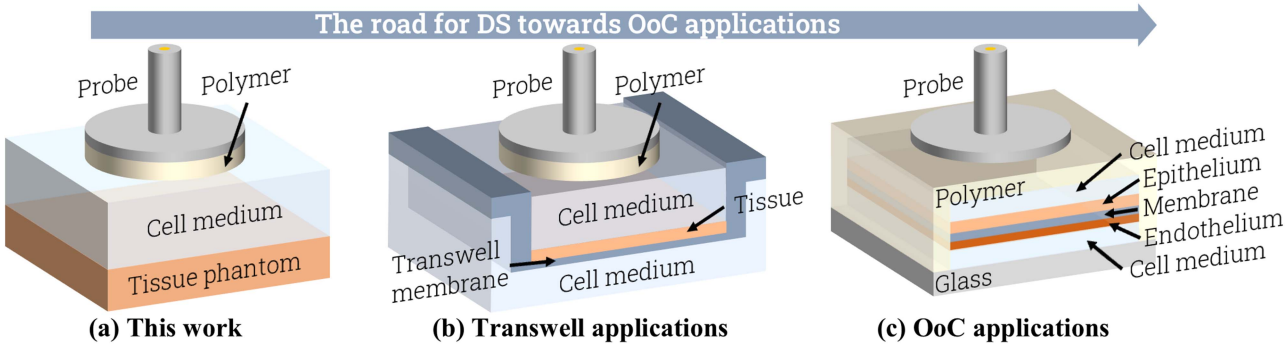

Fig. 1. Envisioned application roadmap toward integration of dielectric spectroscopy in organ-on-chip.

1) Incorporate biocompatible coating to OECPs providing a minimal, well-defined sensitivity loss compared to the non-coated case. This is required given the inclusion of the OECP in the (cell) medium, which would otherwise induce contamination of the medium and corrosion of the OECP surface.
2) Control the height position of the OECP precisely and non-destructively (i.e. by avoiding to touch the tissue in any way) to allow accurate removal of the (thin) cell medium layer and avoid sensitivity losses [20].
3) Employing the spectral analysis-based, high-speed computation tools for OECPs, recently developed by the authors [10], to extract the dieletric properties of a single layer of interest in a stratified (i.e. multi-layered) sample.

In order to present a proof-of-concept of the three key enabling technologies mentioned above, this paper is structured as follows. The Materials and Methods section will provide necessary details of the measurement setup, custom OECP fabrication and coating, and spectrum extraction techniques (bulk and single-layer extraction). Additionally, key elements for micron-accurate height positioning are presented (second key development). In the Results section, OECP DS performance is presented. Firstly, the coated and uncoated OECP performance is compared by measuring various liquids (first key development). These liquids have different dielectric behaviours that have been well-documented by literature, and are also analogous to various tissue types [13], [21], [22]. After, the system's performance for complex multi-layer structures is evaluated (third point from list above). Here, the accuracy of the analytical model is evaluated by comparing it with measurements for 100 different 2-layered compositions. Additionally, the format shown in Fig. 1(a) is presented as a proof-of-concept measurement, where the dielectric properties of a tissue phantom are extracted through a layer of endothelial cell growth medium (ECGM) of various thicknesses. The last sections provide discussion and conclusion, respectively.

II. Materials and Methods

A. Measurement and Characterisation Setup

A custom motorised framework was built to accurately position a sample (in this work, a standard 6-well plate) along the vertical direction (z-axis) with respect to the sensing probe. A

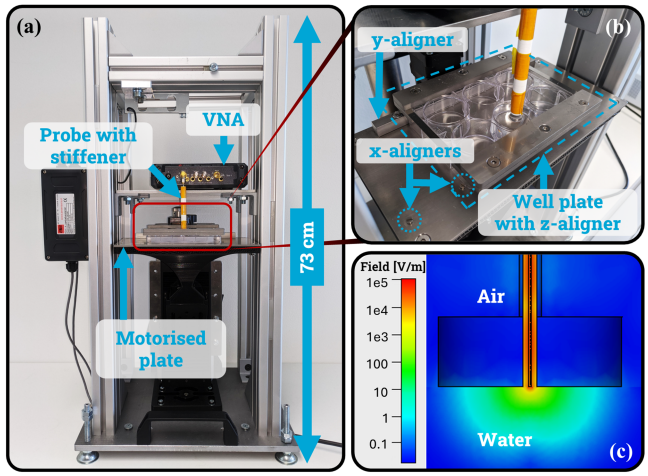

Fig. 2. DS characterisation setup. (a) Full setup, (b) characterisation setup alignment system for 6-well plates, (c) simulated field of a probe. The flange is sufficiently large to confine the electric field to the sample (here: water).

picture of this system can be found in Fig. 2(a). A motorised sample holder (using a 1 μm accurate Thorlabs NRT100 linear motor stage) allows for the positioning of the sample relative to the measurement probe without touching the VNA or the probe, which are very sensitive due to phase and amplitude noise in the measurements. The mechanical stability of the measurement setup is further enhanced by sturdily placing the VNA (Keysight P9374A) on a mounting plate connected to the outer frame and connecting it directly to the probe via a 90° SubMiniature version A (SMA) connector. In addition, the OECP is encapsulated in a 3D-printed PLA stiffener that reduces mechanical movement of the coaxial line.

To ensure that repeated measurements on a well plate are consistently conducted at the same position, the motorised plate was equipped with a 3-axial alignment system (see Fig. 2(b)). This is essential since initial experimental data revealed poor repeatability of measurements due to height variations of the well plate surface (examplified in Figure S1). The aligners reduce these height variations from tens of micrometers to roughly 1 μm, corresponding to the motor stage's repeatability accuracy. It is important to note that, in addition to high positioning reliability, a methodology for absolute height positioning (i.e. a well-defined distance between the probe aperture and the tissue

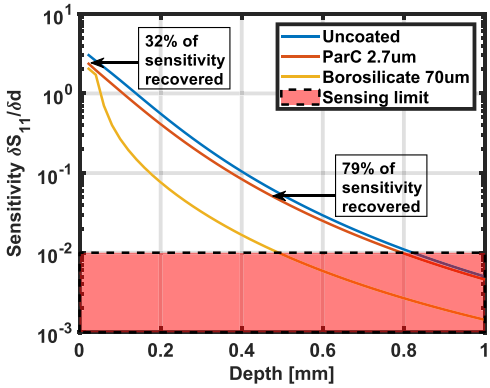

Fig. 3. Simulated probe sensitivity at 10 GHz with different surface finishes. Sensitivity $\delta S_{11}/\delta d$ resembles the change in measured reflectance S_{11} as a function of distance d, where d indicates the thickness of cell medium occupying the space between the probe finish and the tissue phantom (Fig. 1(a)). A percentual performance indicates recovered sensitivity w.r.t. the uncoated probe by opting for Parylene C instead of Borosilicate. At the sensing limit, the sensitivity is no longer distinguishable from sensing noise.

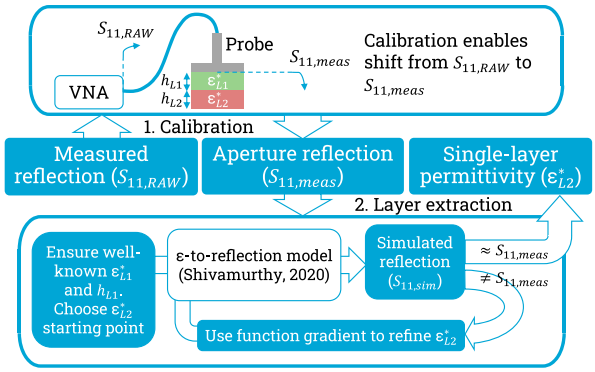

Fig. 4. Simplified data processing flow-chart for single-layer permittivity extraction (here, extracting ϵ^*_{L2}). First, measured data is referred to the probe aperture using probe calibration data. Second, by characterising height and permittivity of intermediate layers in advance (here ϵ^*_{L1}, h_{L1} and h_{L2}), the remaining unknowns (ϵ^*_{L2}) can be extracted by an iterative process.

sample contained in the well plate) is necessary. Such a method is described in Section E of the Materials and Methods section.

B. Custom Open-Ended Coaxial Probes

A custom OECP was manufactured using semi-rigid aluminium coaxial lines (Pasternack SR047AL [23]). The probes were tipped with a flange, which aids in confining the sensing volume to the sample (as seen in Fig. 2(c)) and reduces the complexity in extracting dielectric permittivity data as the effect of the surrounding medium becomes negligible and does not have to be considered [10]. In order to keep the probes compact and easy to handle, the flange width needs not exceed a suitable limit. Using CST Studio Suite, an electromagnetic simulation tool, and assuming water as the device under test (DUT), the flange size was defined such that the simulated electric field strength (Fig. 2(c)) would be below -40 dB at the edge of the flange with respect to the electric field strength at the tip of the coaxial line for all frequencies between 0.1 to 20 GHz. This process resulted in a flange 10 mm in diameter.

Next, the probe was treated with a conformal biocompatible coating to prevent sample contamination and to protect the probe surface. Conventionally, this is done with a borosilicate glass finish [24]. However, with a thickness of at least 70 μm [25], this has a significant impact on the probe's sensitivity (Fig. 3). Conversely, most of the sensitivity can be retained by coating the probe conformally with a much thinner dielectric layer, such as Parylene C (Fig. 3). Compared to glass, Parylene C has the added benefit of having a lower Young's modulus mismatch (more than one order of magnitude) w.r.t. tissue, thus making it more suitable for tissue interaction [26]. As such, a 2.7 μm-thick layer of Parylene C was applied using chemical vapour deposition (CVD) in a remote reactor deposition system (SCS PDS 2010). This thickness was deemed as the smallest which could still ensure conformality and mechanical stability. Parylene C has a complex dielectric permittivity of $3.1 + 0i$ until at least 6 GHz [27] and the permittivity is assumed to be constant across the bandwidth assessed in this work (up to 20 GHz), since this is also the case in similar polymers [28]. It should be noted that a thicker 110 μm polydimethylsiloxane (PDMS)-moulded coating was considered, having similar dielectric properties as Parylene C [29]. However, the increased thickness severely impacted sensitivity (Figure S2) and was thus not further investigated.

C. Permittivity Extraction

Two extraction methods are used in this work. A look-up table (LUT) method can be used as a simple and fast solver [30]. Here, a pre-calculated 3-dimensional table holds S-parameters for a range of viable permittivity-frequency combinations [31]. A searching algorithm can find the closest matching solution of a measurement in this table, where any residual errors due to step sizes are reduced via linear interpolation. Since a LUT assumes a fixed layer composition (number of layers and thicknesses), this method is not suitable if layers regularly change, as a new LUT needs to be generated each time. The LUT-based method is used in this work to convert measurements to a single permittivity spectrum of the entire sensed material (even when the target substrate is actually multi-layered). Such a simplified spectrum is referred to in this work as "homogenised".

To allow for extraction of a single layer's dielectric properties in a multi-layer setting, an iterative solver was developed, as existing work on multi-layer DS is limited to homogenised structures [32]. The solver contains a modified analytical method [10], resulting in the flow-chart found in Fig. 4. This iterative method compares measurement data with data calculated using the analytical model, and tries to optimise the analytical model input using the least-squares solution per frequency point. The method requires well-defined permittivity and absolute height information for most layers in the sample, while up to two of the variables can be left to the solver to be found as an inversion problem (usually ϵ' and ϵ'' of one layer). The method chooses an arbitrary value for the unknown variables as a starting point, and then uses the function gradient

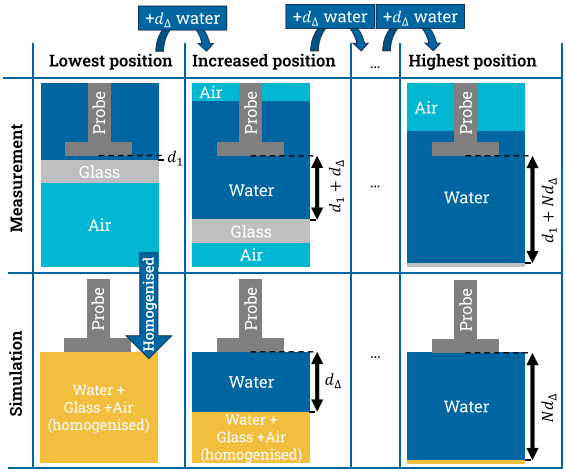

Fig. 5. Simplified diagram showing the material layers in the depth analysis. Probe position is fixed, while the sample's vertical position is changed using the motorised stage (seen in Fig. 2(c)). The lowest simulation position (bottom left figure) has a multi-layer structure with unknowns (e.g. thin film of water between probe and glass of thickness d_1) and is thus substituted with its measured counterpart by assigning the measured homogenised permittivity (using the LUT extraction method) of the lowest position to the initial simulation material. From the lowest position onward, the water layer thickness (between the probe and bottom) of the simulated and measured situation is consistently increased by a specified amount ($d_\Delta = 20\ \mu$m) for N times. At the highest position (rightmost situation), the measurement is no longer distinguishable from an infinitely-thick water layer.

to find a local minimum. Compared to the LUT-based method, this method is computationally roughly 10 times slower.

D. Multi-Layer Characterisation

To characterise the behaviour of the probes in a multi-layered system, a depth sweep analysis was conducted as follows. The dielectric spectrum was measured for a medium (typically water) of varying thickness, backed by some holder (typically glass). When the medium thickness is sufficiently large (i.e. 'highest position' of measurement in Fig. 5), the holder material lies outside of the sensing volume and the measured dielectric spectrum corresponds solely to that of the medium. When the medium thickness is (close to) zero (i.e. 'lowest position' of measurement in Fig. 5), the measured dielectric spectrum is (mostly) that of the holder material. At medium thicknesses where both materials can be sensed, a transitional region is revealed (i.e. 'increased position' of measurement in Fig. 5). Here, the probe is measuring many different multi-layer situations, where two separate materials are measured as a single homogenised material.

Concurrently, the same sweep was simulated via the numerical model [10] as shown in the bottom half of Fig. 5. This simulation assumes two homogeneous layers, where the layer closest to the probe is assumed to be an ideal liquid (usually water) of varying thickness. The dielectric spectrum of the succeeding layer is more complicated to characterise. In fact, the backing includes air as well as glass since the glass has finite thickness. Additionally, even when the probe is as close as possible to the glass, a very thin layer of water remains between the probe and the glass surface due to surface imperfections and misalignment. To circumvent the need to accurately characterise this multi-material composite, a homogenised spectrum was measured and used in the simulation environment. This is the (probe level calibrated) reflectometry data where the probe is closest to the glass holder, effectively measuring a thin layer of water, followed by the glass holder and backed by air (shown in the 'lowest position' situation in Fig. 5). Using the experimental data of the simulation composite layer, we enforced that the measured and simulated data have identical spectra at a water height of 0 μm.

The depth sweep analysis allows the extraction of three probe performance metrics. Firstly, an estimated error between measured multi-layer data and equivalent simulated data, indicating model mismatch, calculated using the formula:

$$error = \left| \frac{\epsilon^*_{meas} - \epsilon^*_{sim}}{\epsilon^*_{sim}} \right| * 100\% \qquad \forall \epsilon^* \in \mathbb{C} \qquad (1)$$

where ϵ^*_{meas} and ϵ^*_{sim} are the LUT-extracted complex permittivity data of the measured and simulated datasets, respectively. Secondly, measured data S_{11} is derived over depth d to extract the sensitivity metric $\delta S_{11}/\delta d$, which shows a sensing depth profile when plotted. For the first and second metric, an uncoated probe was used. For the third metric, i.e. the single-layer extraction performance, the measurement was repeated in a more biological setting. Here, a Parylene C-coated probe was used in a 6-well plate (polycarbonate) containing endothelial cell growth medium (ECGM). The first material layer had a well-defined thickness (10, 20, 50, 100 or 150 μm) and consisted solely of ECGM. Similar to before, the second layer is a multi-material layer consisting of air, plastic and a thin slice of ECGM. However, here, the ECGM slice thickness was chosen such that the homogenised permittivity ϵ' of this second layer composite is roughly 20 at 500 MHz and 10 at 20 GHz, thus allowing the second layer composite to act as a phantom material with dielectric properties similar to e.g. bladder and lung tissue [21]. After characterising the dielectric properties of ECGM, the iterative permittivity extraction for single layers is used to omit the effect of the intermediate ECGM layer. The extracted complex permittivity of the biological phantom can then be compared with a reference measurement conducted at the surface of the biological phantom. The process is repeated for the different ECGM layer thicknesses.

E. Absolute Height Calibration

For all the multi-layer characterisation measurements, it is essential to have a well-defined distance between the probe's aperture surface and the sample surfaces and/or interfaces. Therefore, we define $d = 0$ as the lowest probe position where the permittivity does not vary (outside the trace noise limit). When inserting the probe in a well with different absolute height, the S_{11} magnitude and phase response can be used as an aligner using the depth sweep analysis described in the previous section. Additionally, when the aligners in Fig. 2(b) are used, the height position can be saved such that this absolute height calibration is only required once per well. As such, more generally, this height referencing technique can be used for non-contact measurements with tissue if a depth sweep analysis is conducted on the well

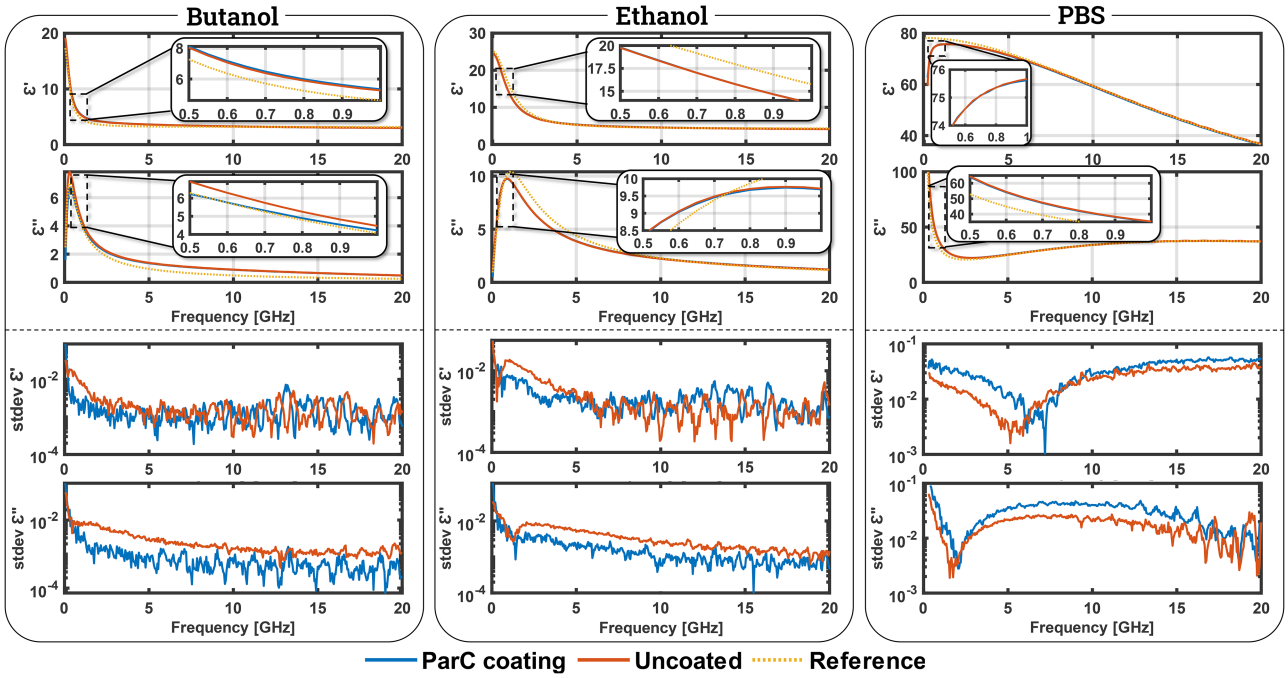

Fig. 6. Complex dielectric spectrum comparison between Parylene C-coated (blue lines) and uncoated (red lines) probes and reference (yellow dotted lines). Note that some measurement datasets are highly correlated; some coated probe data is concealed behind the uncoated probe data. LTR: the top graphs show the real and imaginary spectra of butanol, ethanol and PBS. Corresponding with the top graph's liquids, the bottom graphs show real and imaginary spectral standard deviations due to VNA noise (5 measurements each).

before cell seeding (the well's surface cannot be reached in presence of cells).

III. Results

A. Non-Contact Sensing Through Parylene C

Using an uncoated probe and a Parylene C-coated probe, various liquids were measured and converted to a dielectric spectrum using the LUT method. Measurement liquids compared in this work are analogous to tissues: butanol to fat, ethanol to breast tissue and PBS to culturing medium [13]. Permittivity results can be found in the top half of Fig. 6.

As shown in Fig. 3, minimal sensitivity loss is expected for coated probes. To compare the sensitivity performance of the coated and uncoated probe, the spectrum measurements were repeated fivefold in order to calculate the standard deviation and thus reveal measurement dispersion due to VNA noise. These data are presented in the lower half of Fig. 6 and indicate that the coated probe's performance is indeed similar to that of the uncoated probe. In fact, there is no consistent difference in noise-related spread when considering data of all three measurements.

B. Multi-Layer Permittivity Extraction Accuracy

Three probe performance metrics were investigated for multi-layer permittivity extraction. Firstly, the probe's sensitivity through water as a function of distance is presented in Fig. 7(a), indicating a maximum sensing depth of about 1 to

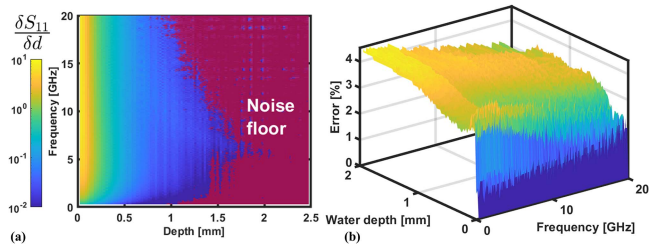

Fig. 7. Probe performance data. (a) Probe sensitivity as a function of frequency and depth using an uncoated probe, where the dark-red region indicates the probe's limit of detection due to VNA noise, (b) Percentual error between measured and simulated depth-sweep data through DI water and a glass backing material, calculated according to (1).

1.5 mm depending on the field's frequency. Secondly, correspondence of the depth sweep measurement and its numerically-simulated analogue can be seen in Fig. 7(b), showing an estimated error percentage that is fairly consistently between 3 to 4 %. In both figures, the step size for depth is 2 μm, hence 100 different situations were analysed.

Finally, an OoC-analogous setup as shown in Fig. 1(a) was used to demonstrate single-layer extraction of a tissue phantom with an intermediate ECGM layer of various thicknesses. These results can be found in Fig. 8. When compared with the tissue phantom reference, the homogenised results (top graphs in Fig. 8) show a striking impact on the measured spectrum due to the intermediate ECGM layer, even for smaller ECGM layer thicknesses (up to 150 μm). To counter this effect, the permittivity of ECGM was characterised separately so that the presented iterative extraction method can be used. The result

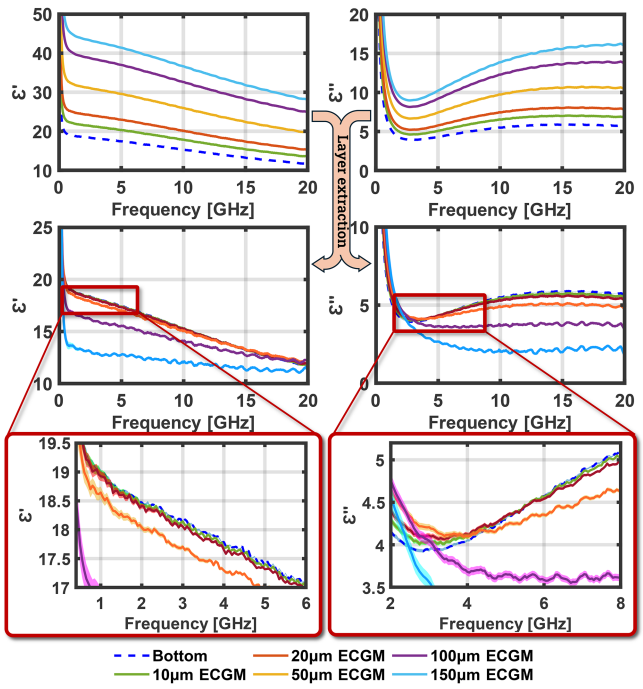

Fig. 8. Processed multi-layer spectral data. Top graphs show the sample's homogenised spectra (i.e. ECGM and tissue phantom), while the remaining graphs show the extracted spectra of the tissue phantom only (removing the effect of the intermediate ECGM layer). The dashed blue indicates the biological phantom and thus acts as a measurement reference. Graphs on the left and right respectively show the real part (ϵ') and imaginary part (ϵ'') of the permittivity.

is a largely recovered tissue phantom permittivity (middle and bottom graphs in Fig. 8), especially for the cases with thinner ECGM layers.

IV. Discussion

A. Reference Deviation

Although the permittivity data presented in Fig. 6 is largely overlapping, both measurements deviate from the reference curve. This offset is most likely caused by systematic differences between the simulated reference and the measurement, such as liquid impurities (calibration and characterisation liquids), temperature offsets (reference assumes 20 °C) and manufacturing inconsistencies (e.g. probe surface roughness or coaxial line centrocity). A quantification of these errors can be extracted following a recently developed extraction procedure [33], where minimisation of the highest contributing source should be prioritised. Ideally, an application-resembling environment should be analysed here (e.g., closed-loop temperature control at 37 °C using a tissue incubator).

B. Single-Layer Extraction

Fig. 8 shows that the extraction of the tissue phantom material works especially well for thin ECGM layers, but that there is an apparent bias for thicker ECGM layers. Although the phantom is clearly still in the sensing region of the probe (according to Fig. 7(a)), it should be noted that sensitivity reduces as a function of the ECGM layer thickness, which can result in the observed bias. In fact, observing the data presented in Fig. 7(a) reveals that sensitivity is reduced more than fivefold at 10 GHz over the first 150 μm closest to the OECP surface. Additionally, imperfect characterisation of the ECGM layer's permittivity spectrum can be a contributor to the observed bias. Therefore, even when materials are still within the sensing region of the OECP, it is preferred to have the material of interest as close as possible to the sensing surface if high sensitivity is required. Regardless, further technological development is required to improve extraction capabilities through thicker intermediate materials.

V. Conclusion

This work evaluated the feasibility of DS in OoC applications using OECPs. To facilitate this, we manufactured a characterisation and alignment setup, as well as custom Parylene C-coated OECPs. Furthermore, we described a precise repeatable positioning and single-layer extraction procedure. This paper presents three key technological developments in order to confirm functionality of DS in OoC.

The first development focussed on the non-contact aspects of DS by applying a 2.7 μm-thick surface coating of Parylene C. We expected that the sensitivity of these OECPs would be somewhere between borosilicate-coated and uncoated OECPs (Fig. 3). Surprisingly, however, measurement data showed measurement performance indistinguishable to uncoated probes (Fig. 6), thus indicating that the Parylene C coating has no significant impact on probe performance.

The second development required a methodology to reliably determine the distance to stratifications in a multi-layered sample without touching the material interface, potentially disrupting the tissue surface. We devised an enabling height calibration technique to accurately and reliably position the OECP with respect to the sample. If this procedure is conducted before cell seeding, the position of the OECP can be set at a specified distance to the cells with 1 μm accuracy without touching the tissue surface. Due to height variations of well plates, this height accuracy can only be achieved by means of high placement repeatability, for which we successfully developed a three-axial alignment system (Fig. 2(b)).

This accurate height positioning additionally enabled the last key technological development, focussed on the potency of measuring multi-layered materials. Firstly, we compared the analytical model, used for single-layer extraction, with measured data. This showed close resemblance ($3-4\,\%$ deviation shown in Fig. 5(b)) and thus proved the model's ability to capture the essence of multi-layered structures. Secondly, we determined probe sensitivity as a function of distance, which showed a sensing depth of roughly $1-1.5$ mm for an uncoated OECP (Fig. 7(a)). Lastly, we proved, with a proof-of-principle measurement on a tissue phantom material, that single-layer spectral data can be recovered accurately through a layer of ECGM of various thicknesses, particularly when the OECP is positioned close to the layer of interest (Fig. 8).

This paper has shown the considerable potential of DS in OoC and some of its limitations. The technique can reliably extract single-layer tissue phantom data requiring neither tissue nor cell

medium contact. Future work must identify which cell processes can be tracked with DS. Since the setup is optimised for well plates, a transwell (Fig. 1(b)) can be a drop-in replacement for tissue investigation. Ideally, this would require a better understanding of the sensing accuracy and setup parameters such as VNA noise, coating composition, calibration accuracy and temperature. Furthermore, for DS to succeed in the OoC domain, microfluidic integration is needed which would require integration of a DS antenna (Fig. 1(c)). Such a system would simplify alignment of biological tissue to the sensing surface, aiding in accurate multi-layer spectral extraction in complex tissue. Looking beyond OoC, the presented work could be adapted for other non-invasive applications with stratified interfaces, such as food/drug quality monitoring, bioreactors and skin inspection.

ACKNOWLEDGMENT

The authors would like to thank for all the technical support received to make this project possible, particularly from the people from the Else-Kooi Lab (EKL), Dienst Elektronische en Mechanische Ontwikkeling (DEMO), Delft High Performance Computing Centre (DHPC) and Leiden University Medical Centre (LUMC). Specifically, Sjoerd de Jong for his aid in data processing, Juan Bueno Lopez for his support in the labs and Merve Bulut for her input on biological relevance. In addition, thank you OoC group for your valuable feedback and insightful contributions during the weekly feedback meeting.

REFERENCES

[1] P. Mehrotra, B. Chatterjee, and S. Sen, "EM-Wave biosensors: A review of RF, microwave, mm-wave and optical sensing," *Sensors*, vol. 19, no. 5, Feb. 2019, Art. no. 1013.

[2] D. Q. M. Craig, *Dielectric Analysis of Pharmaceutical Systems*, 1st ed. London, U.K.: Taylor & Francis, 1995.

[3] W. H. H. Woodward, "Broadband dielectric spectroscopy—a practical guide," in *Broadband Dielectric Spectroscopy: A Modern Analytical Technique*(ACS Symp. Ser.), W. H.H. Woodward, Ed. Washington, DC, USA: Amer. Chem. Soc., Jan. 2021, vol. 1375, pp. 3–59.

[4] C. Polk and E. Postow, *Handbook of Biological Effects of Electromagnetic Fields, -2 Volume Set*. Boca Raton, FL, USA: CRC Press, 1995.

[5] K. Heileman, J. Daoud, and M. Tabrizian, "Dielectric spectroscopy as a viable biosensing tool for cell and tissue characterization and analysis," *Biosensors Bioelectron.*, vol. 49, pp. 348–359, Nov. 2013.

[6] P.-O. Bagnaninchi, M. Dikeakos, T. Veres, and M. Tabrizian, "Complex permittivity measurement as a new noninvasive tool for monitoring in vitro tissue engineering and cell signature through the detection of cell proliferation, differentiation, and pretissue formation," *IEEE Trans. Nanobiosci.*, vol. 3, no. 4, pp. 243–250, Dec. 2004.

[7] M. Mertens, M. Chavoshi, O. Peytral-Rieu, K. Grenier, and D. Schreurs, "Dielectric spectroscopy: Revealing the true colors of biological matter," *IEEE Microw. Mag.*, vol. 24, no. 4, pp. 49–62, Apr. 2023.

[8] V. Technologies and B.V., "FRESCO handheld sensor for flexible quality control of fresh fruits," 2024. Accessed: Jan. 18, 2024. [Online]. Available: https://mcusercontent.com/2cdc18a8f92ed7584bcf3af8c/files/deebcdf6-b93a-4e17-c48d-1af8c7741dbe/FMS_H_brochure_front_Jan]_year2024.pdf

[9] H. T. Shivamurthy, Z. Hu, G. Vlachogiannakis, M. Spirito, and A. Neto, "Equivalent circuit modeling of a single-ended patch sensing element in integrated technology," *IEEE Trans. Microw. Theory Techn.*, vol. 68, no. 1, pp. 17–26, Jan. 2020.

[10] H. T. Shivamurthy, "On the design and analysis of micro-metric resolution arrays in integrated technology for near-field dielectric spectroscopy," Ph.D. dissertation, Delft University of Technology, Delft, Feb. 2020.

[11] E. Fear, S. Hagness, P. Meaney, M. Okoniewski, and M. Stuchly, "Enhancing breast tumor detection with near-field imaging," *IEEE Microw. Mag.*, vol. 3, no. 1, pp. 48–56, Mar. 2002.

[12] F. Artis et al., "Microwaving biological cells: Intracellular analysis with microwave dielectric spectroscopy," *IEEE Microw. Mag.*, vol. 16, no. 4, pp. 87–96, May 2015.

[13] A. La Gioia et al., "Open-ended coaxial probe technique for dielectric measurement of biological tissues: Challenges and common practices," *Diagnostics*, vol. 8, no. 2, Jun. 2018, Art. no. 40.

[14] C. Aydinalp, S. Joof, I. Dilman, I. Akduman, and T. Yilmaz, "Characterization of open-ended coaxial probe sensing depth with respect to aperture size for dielectric property measurement of heterogeneous tissues," *Sensors*, vol. 22, no. 3, Jan. 2022, Art. no. 760.

[15] D. M. Nahon et al., "Standardizing designed and emergent quantitative features in microphysiological systems," *Nature Biomed. Eng.*, vol. 8, no. 8, pp. 941–962, Aug. 2024.

[16] M. Schlander, K. Hernandez-Villafuerte, C.-Y. Cheng, J. Mestre-Ferrandiz, and M. Baumann, "How much does it cost to research and develop a new drug? A systematic review and assessment," *Pharmaco Econ.*, vol. 39, no. 11, pp. 1243–1269, Nov. 2021.

[17] L. A. Low, C. Mummery, B. R. Berridge, C. P. Austin, and D. A. Tagle, "Organs-on-chips: Into the next decade," *Nature Rev. Drug Discov.*, vol. 20, no. 5, pp. 345–361, May 2021.

[18] M. Mastrangeli and J. van den Eijnden-van Raaij, "Organs-on-chip: The way forward," *Stem Cell Reports*, vol. 16, no. 9, pp. 2037–2043, Sep. 2021.

[19] S. Fuchs, S. Johansson, A. Ø. Tjell, G. Werr, T. Mayr, and M. Tenje, "In-Line analysis of organ-on-chip systems with sensors: Integration, fabrication, challenges, and potential," *ACS Biomaterials Sci. & Eng.*, vol. 7, no. 7, pp. 2926–2948, Jul. 2021.

[20] A. Fallahi, S. Hashemizadeh, and N. Kuster, "On the dielectric measurement of thin layers using open-ended coaxial probes," *IEEE Trans. Instrum. Meas.*, vol. 70, 2021, Art. no. 6011808.

[21] S. Gabriel, "Appendix c: Modelling the frequency dependence of the dielectric properties to a 4 dispersions spectrum," Jun. 1997. Accessed: Mar. 20, 2024. [Online]. Available: http://niremf.ifac.cnr.it/docs/DIELECTRIC/AppendixC.html

[22] A. P. Gregory and R. N. Clarke, "Tables of the complex permittivity of dielectric reference liquids at frequencies up to 5 GHz," Report/Guide MAT 23, Jan. 2012.

[23] Pasternack Enterprises Inc, "047 semi-rigid coax cable with tinned aluminum outer conductor," 2023. Accessed: Jan. 15, 2024. [Online]. Available: https://www.pasternack.com/images/ProductPDF/PE-SR047AL-STRAIGHT.pdf

[24] A. Mirbeik-Sabzevari and N. Tavassolian, "Characterization and validation of the slim-form open-ended coaxial probe for the dielectric characterization of biological tissues at millimeter-wave frequencies," *IEEE Microw. Wireless Compon. Lett.*, vol. 28, no. 1, pp. 85–87, Jan. 2018.

[25] S. Borofloat, "The versatile floated borosilicate glass - with an infinite number of applications," Accessed: Sep. 11, 2024. [Online]. Available: https://www.pegasus-glass.com/Portals/0/Borofloat.pdf

[26] K. Scholten and E. Meng, "Materials for microfabricated implantable devices: A review," *Lab Chip*, vol. 15, no. 22, pp. 4256–4272, 2015.

[27] VSi Parylene, "The complete guide to parylene properties: A comprehensive guideline to determining Parylene's applicability to your project," May 2020 Accessed: Dec. 08, 2023. [Online]. Available: https://www.vsiparylene.com/wp-content/uploads/2020/05/VSI-Parylene-Complete-Guide-to-Parylene-Coatings-Digital.pdf

[28] S. Sahin, N. K. Nahar, and K. Sertel, "Dielectric properties of low-loss polymers for mmW and THz applications," *J. Infrared, Millimeter, Terahertz Waves*, vol. 40, no. 5, pp. 557–573, May 2019.

[29] H. Shivashankar, A. Kevin, S. Manohar, and S. Kulkarni, "Investigation on dielectric properties of PDMS based nanocomposites," *Physica B: Condens. Matter*, vol. 602, Feb. 2021, Art. no. 412357.

[30] T. Hosman, M. Mastrangeli, and M. Spirito, "Dielectric spectroscopy for non-invasive sensing of multi-layered organ-on-chip devices," *Proceedings*, vol. 97, Mar. 2024, Art. no. 23.

[31] Delft high performance computing centre (DHPC), DelftBlue supercomputer (phase 1)," 2022. [Online]. Available: https://www.tudelft.nl/dhpc/ark:/44463/DelftBluePhase1

[32] R. Irastorza, M. Mayosky, and F. Vericat, "Noninvasive measurement of dielectric properties in layered structure: A system identification approach," *Measurement*, vol. 42, no. 2, pp. 214–224, Feb. 2009.

[33] T. B. Hosman, E. Shokrolahzade, M. Mastrangeli, and M. Spirito, "Numerical testbench for a priori uncertainty estimation of dielectric spectroscopy in organ-on-chip devices," in *IEEE MTT-S IMS*, San Fransisco, in press, Jan. 2025.

Tim Hosman received the B.Sc. degree in electrical engineering and the M.Sc. degree in microelectronics, from the Delft University of Technology (Delft, NL) in 2016 and 2020, respectively. He is currently a Ph.D. Candidate in a collaborative project between Electronic Components, Technology, and Materials and Electronic Circuits and Architectures within the Microelectronics Department, Delft, NL. He has worked on various biomedical research projects, including a flexible neuro-implantable (Fraunhofer IZM, Berlin, DE), a wearable ultrasound patch (ULIMPIA, Delft, NL) and an exoskeleton (Project MARCH, Delft, NL). His research interests include implementing dielectric spectroscopy as a novel sensing technique for organs-on-chip applications.

Massimo Mastrangeli (Member, IEEE) received the B.Sc. and M.Sc. degrees (cum laude) in electronic engineering from University of Pisa, Pisa, Italy, and the Ph.D. degree in materials engineering from University of Leuven, Leuven, Belgium. He is an Associate Professor in the Electronic Components, Technology and Materials section of the Microelectronics Department of Delft University of Technology, Delft, The Netherlands, where he is developing innovative microelectromechanical organ-on-chip devices and platforms. He held Research Positions with École Polytechnique Fédérale de Lausanne (EPFL, CH), Université Libre de Bruxelles, Brussels, Belgium and Max Planck Institute for Intelligent Systems, Stuttgart, Germany. He is also a Guest Lecturer with EPFL and Board Member of the European Organ-on-Chip Society.

Marco Spirito (Member, IEEE) received the M.Sc. (*cum laude*) degree in electrical engineering from the University of Naples Federico II, Naples, Italy, in 2000, and the Ph.D. degree in microelectronics from TU Delft, Delft, The Netherlands in 2005. In 2008, he was with the ELCA research group, TU Delft University where he has been an Associate Professor since 2013. In 2010 and 2017, he was one of the co-founders of Anteverta-MW, and Vertigo Technologies, respectively. Dr. Spirito was the recipient of the IEEE Microwave Theory and Techniques Society Microwave Prize in 2008. He was a co-recipient of the Best Student Paper Award at the 2011 IEEE RFIC Symposium, the GAAS Association Student Fellowship in 2012, the Best Student Paper Award in second place at the 2018 IMBioC, the Best Paper Award at the 2019 Winter ARFTG Conference, and the Best Student Paper Award at the 2019 Summer ARFTG Conference.